Available online at www.sciencedirect.com
SCIENCE DIRECT®
Journal of Nuclear Materials 355 (2006) 89–103
journal of nuclear materials
www.elsevier.com/locate/jnucmat

Dependence of radiation damage accumulation in iron on underlying models of displacement cascades and subsequent defect migration

A. Souidi [a,1], C.S. Becquart [b], C. Domain [c], D. Terentyev [d], L. Malerba [d], A.F. Calder [e], D.J. Bacon [e], R.E. Stoller [f], Yu. N. Osetsky [g], M. Hou [a,*]

[a] *Physique des Solides Irradiés et des Nanostructures CP234, Université Libre de Bruxelles, Boulevard du Triomphe, B-1050 Brussels, Belgium*
[b] *Laboratoire de Métallurgie Physique et Génie des Matériaux, UMR 8517, Université de Lille-1, F-59655 Villeneuve d'Ascq cédex, France*
[c] *EDF-R&D Département MMC, Les renardières, F-77818 Moret sur Loing cédex, France*
[d] *SCK•CEN, Reactor Materials Research Unit, B-2400 Mol, Belgium*
[e] *Department of Engineering, The University of Liverpool, Liverpool L69 3GH, England, UK*
[f] *Metals and Ceramics Division, Oak Ridge National Laboratory, Oak Ridge, TN, USA*
[g] *Computer Science and Mathematics Division, Oak Ridge National Laboratory, Oak Ridge, TN, USA*

Received 3 February 2006; accepted 24 April 2006

Abstract

Groups of displacement cascades calculated independently with different simulation models and computer codes are compared on a statistical basis. The parameters used for this comparison are the number of Frenkel pairs (FP) produced, the percentages of vacancies and self-interstitial atoms (SIAs) in clusters, the spatial extent and the aspect ratio of the vacancies and the SIAs formed in each cascade. One group of cascades was generated in the binary collision approximation (BCA) and all others by full molecular dynamics (MD). The MD results differ primarily due to the empirical interatomic potentials used and, to some extent, in code strategies. Cascades were generated in simulation boxes at different initial equilibrium temperatures. Only modest differences in the predicted numbers of FP are observed, but the other cascade parameters may differ by more than 100%. The consequences of these differences on long-term cluster growth in a radiation environment are examined by means of object kinetic Monte Carlo (OKMC) simulations. These were repeated with three different parameterizations of SIA and SIA cluster mobility. The differences encompassed low to high mobility, one- and three-dimensional migration of clusters, and complete immobility of large clusters. The OKMC evolution was followed until 0.1 dpa was reached. With the range of OKMC parameters used, cluster populations after 0.1 dpa differ by orders of magnitude. Using the groups of cascades from different sources induced no difference larger than a factor of 2 in the OKMC results. No correlation could be identified between the cascade parameters considered and the number densities of vacancies and SIAs predicted by OKMC to cluster in the long term. However, use of random point defect distributions instead of those obtained for displacement cascades as input for the OKMC modeling led to significantly different results.

* Corresponding author. Tel.: +32 2 6505735; fax: +32 2 6505227.
E-mail address: mhou@ulb.ac.be (M. Hou).
[1] Present address: Centre Universitaire Dr. Moulay Tahar de Saida, BP138 En Nasr, Saida 20000, Algeria.

doi:10.1016/j.jnucmat.2006.04.009

It is therefore suggested that although the displacement cascade characteristics considered do not correlate with cluster populations in the long term, other aspects of the internal structure of cascades do.

PACS: 61.80.Az; 61.82.Bg; 61.80.Hg; 34.20.Cf

1. Introduction

The evolution of damage in a radiation environment spans several spatial and time scales and it is a substantial challenge to predict the long-term mechanical property changes in materials induced by radiation. For this purpose, one approach consists of chaining together existing models at different scales covering phenomena that range from the recoiling of atoms induced by irradiating particles to the macroscopic defective state of the material [1]. At the atomic scale, collision cascade generation by primary recoils in metals, the subsequent partial recovery and the evolution toward the resulting point defect distributions can be naturally simulated by molecular dynamics (MD). In metals, and thus in iron on which the present report focuses, point defects in displacement cascades are inhomogeneously distributed and may spontaneously form small clusters. They evolve over long times for which MD modeling turns out to be impractical. To overcome this limitation, MD may be chained with a kinetic Monte Carlo (KMC) simulation that describes the thermal evolution of point defects and point defect clusters up to the mesoscopic scale. Since cluster thermal mobility and diffusion mechanisms depend on their size and type, different diffusion models need to be applied to each of them. The object KMC (OKMC) method allows different diffusion properties to be attributed to different objects and is therefore suitable for this type of study.

Both MD and OKMC models are constructed on the basis of strategies for limiting the necessary computational effort and of parameters subtending the models. For these reasons, predictions are to some extent approximate. One thus has to face the double problem of estimating both the degree of approximation inherent to one scale (here the atomic scale) and the propagation of approximations when moving to larger scales (here the mesoscopic scale). A way to tackle this problem is to compare predictions from different models and computational strategies and to measure directly the consequences of their differences at the next scale. The purpose of the collective exercise presented in this report is to estimate the magnitude of differences in predictions made at the atomic scale by independent MD approaches, and to measure their consequences for the results of OKMC predictions at the mesoscale while using different parameterizations of the OKMC model. The complete MD simulation of displacement cascades is computationally demanding, and a number of cascades must be completed at any one energy/temperature condition to permit a valid statistical comparison of different potentials and MD models. During more than a decade, the authors of this report produced studies and reviews of various aspects of damage production in iron at the atomic scale using different codes and models and, more recently, up to the mesoscopic scale using OKMC [2–38]. In this report, the results of the simulations performed independently over the last decade are used to estimate the magnitude of differences in atomic scale predictions on a statistical basis and the consequences on the long-term defect cluster growth using different parameterizations of the OKMC.

The paper is organized as follows. Section 2 describes the methodology used for the atomic scale and OKMC damage predictions. Models and code strategies used are summarized in Section 3 (more complete detail is available in the literature). Section 4 describes the cascade analysis methods. Section 5 provides a comparison of cascade results gathered by the different participating groups and Section 6 examines the possible consequences of primary damage on the longer term evolution in a radiation environment by means of OKMC with three different sets of parameters describing SIA defect mobility. The results are discussed in Section 7.

2. Methodology

2.1. Displacement cascades

The displacement cascades used were produced in models of alpha-iron with four different codes. The first three are full MD codes that were developed

independently. MOLDY [39] (labeled 'MLD' in what follows) was used for modeling cascades generated by primary recoil atoms with kinetic energies in the range of 0.1–200 keV; DYMOKA [15] (labeled 'DMK' in what follows) was used for cascades in the 5–30 keV range; and LIVCAS [16] (labeled 'LVP' in what follows) was used for cascades in the 1–25 keV range. The fourth code, MARLOWE [40], uses the binary collision approximation of MD, to permit fast computation of collision cascades and was implemented by an approximate treatment of short-term point defect recombination in order to bridge the collisional (ballistic) phase to the displacement cascade [24]. It is labeled 'BCA' in what follows. In order to present the largest possible comparison, given the results available, 5, 10 and 20 keV cascades are analyzed here. We consider the mean numbers of point defects and the mean fractions of clustered vacancies and SIAs produced per cascade. Longer-range correlations are estimated and compared by means of pair distance correlation functions and mean spatial cascade extensions and aspect ratios are also estimated and compared. In order to avoid the risk of different results originating from different definitions and analysis protocols, the same analysis algorithms are used for all sets of cascades computed by each participating research team.

2.2. The long term point defect cluster growth

To our knowledge, there are only a few OKMC codes presently available, the most popular being BigMac [41,42] and LAKIMOCA [31]. We use the latter. Quantitative OKMC predictions are dependent on the parameters used for describing the mobility of point defects and their clusters [38,43]. Different sets of parameters were discussed in [31] and this discussion is not repeated here. Instead, the different sets of displacement cascades available are used as OKMC input and the OKMC results compared at given OKMC conditions. Repeating the OKMC simulations with the three parameters sets described below allows differentiation of the contribution of the primary damage and the OKMC models to any variability in the OKMC results. Defect data for cascades generated in model simulation boxes initially set at two different temperatures 100 K and 600 K are employed so that, by using one constant temperature in the OKMC simulations, the effect of cascade temperature on the long-term defect cluster populations can be determined.

3. The displacement cascades and the OKMC models

3.1. The displacement cascades

The sets of cascades analyzed and used for long term predictions are given in Table 1, in terms of simulated energies and temperatures, as well as codes and potentials used. As a whole, it represents 262 full MD cascades and 6000 BCA cascades. The properties of the different interatomic potentials used [59–65] have been partially reviewed in the literature [15,37,44], and compared with experimental and ab initio results [46–58]. Among these potentials, produced over the last 20 years, the one recently derived by Ackland and co-workers [59], here denoted as AMS, is currently considered to be the most accurate of all, since it was fitted to reproduce the formation energy of SIA configurations as obtained by ab initio calculations [45] and verified to provide migration energies in accordance with both experimental and ab initio results [68].

The full MD simulations are characterized by

(1) *The equilibrium interatomic potentials*. Six different equilibrium potentials were employed in the full MD simulations, and are discussed in the references cited.
(2) *The short range pair potential branches*. For close encounters between atoms, the repulsive

Table 1
Numbers of cascades used as generated with each code

	5 keV		10 keV		20 keV	
	100 K	600 K	100 K	600 K	100 K	600 K
LVP (AMS [59])	30	36	30	30	10	20
MLD (FS [60])	9		15		10	8
DMK (SP [61])		5		5		4
DMK (ABC [62])					10	
DMK (AMS)					10	
DMK (CWP [63])					10	
DMK (WOL [64])					10	
BCA (ZBL [65])	1000	1000	1000	999	1000	1000

The potentials are given in parenthesis. Cascades are regrouped according to the primary recoil energy and the initial temperature of the simulation boxes.

pair component of each equilibrium potential is joined to the screened Coulomb potential in [65] by means of a cubic spline. The spline nodes differ from one potential to the other. The potential in [65] is also employed in the BCA simulations.

(3) *The simulation box sizes*. The MD simulation boxes are all cubic in shape, but the sizes used differ from one set of simulations to another. LVP simulation box sizes range from 50 to $100a_0$ (250 000 to two million atoms) for cascades from 5 to 20 keV, where a_0 is the lattice parameter. MLD box sizes range from 30 to $60a_0$ (54 000 to 432 000 atoms) in the same energy range. The box sizes employed for generating DMK cascades ranged from 50 to $80a_0$ (250 000–1 024 000 atoms).

(4) *The boundary conditions*. Periodic boundary conditions are used in three codes. LVP and DMK simulations were carried out at constant volume, while in MLD the boundaries of the simulation are maintained at constant (zero) pressure [60]. In all three cases the simulation boxes are thermally isolated, leading to an increase of the temperature due to the kinetic energy of the primary knock on atom. This increase depends on the box size and may be estimated as of the order of $\Delta T = \widehat{E}/3Nk_B$ where $\widehat{E}$ is the part of the cascade energy which is not spent in the production of permanent defects, k_B the Boltzman constant and N the number of atoms in the box.

(5) *The time step and the duration of the cascade evolution*. For the DMK cascades, the simulation was broken into a number of time segments and a constant time step was used in the integration of the equations of motion during each segment. The duration of the various segments was determined by the kinetic energies of the moving atoms and the time step in each segment was adjusted accordingly. The MLD and LVP cascades were generated using a multiple time step that adjusted automatically according to the kinetic energy of moving particles so as to limit either the maximum energy change or the maximum atom movement during a timestep [16,39]. The LVP code further optimized performance by using effectively longer timesteps in regions of the box where the kinetic energy of the atoms was undisturbed by the cascade event. The cascade event was considered to be over when all of the initial kinetic energy of the primary recoil was thoroughly dissipated and atom motion was controlled by simple thermal oscillations.

In the BCA method, the equations of motion are not integrated stepwise in time. The MARLOWE code offers several options for modeling collision cascades and, in brief, the model selected here is as follows. Collision cascades are modeled as sequences of binary encounters between a projectile and a target atom at rest. The latter can either be a lattice atom or an already-stopped recoil. Multiple interactions are only treated approximately, imposing momentum conservation and subsequent rescaling of the velocities. Between collisions, atoms are considered to follow their asymptotic path. The position of the asymptotes as well as the elastic energy transfers are deduced from the scattering integrals, namely, the scattering angle in the centre of mass system and the time integral, according to [40]. For consistency with the full MD cascades described above, the ZBL interaction potential is chosen. A clock is assigned to each moving particle and is incremented at each collision with the collision time deduced from the time integral. Moving atoms are ordered into time-slabs and those in the earliest slab are selected for the next collision until this slab is empty, and so on. Except in the case of replacement collisions to which a specific treatment is applied (see [25,26,36] for a discussion in the case of iron), target atoms are assumed bound to their lattice sites with an energy equal to the cohesive energy of iron. Such recoils are then identified as cascade atoms if their kinetic energy at the exit of their collisions is higher than a threshold value. A trajectory calculation is stopped when the kinetic energy of a moving atom falls below a cut-off value, here chosen equal to the displacement energy threshold which is close to the cohesive energy of iron. This threshold is a calculational parameter which has no relation with the threshold energy for producing a stable Frenkel pair. In the present model, non-replacing atoms stopped at the cut-off energy are considered as nascent interstitials, candidates for the formation of Frenkel pairs. In order to determine stable Frenkel pairs, each nascent interstitial is paired to its closest vacancy. The defects are only retained as a Frenkel pair if their separation is larger than a specified recombination distance which is used as a parameter. In the results presented below, this parameter is adjusted in such

a way that the number of Frenkel pairs produced in 10 keV cascades is the same as predicted by full MD with the DMK (SP) (see Table 1).

3.2. The OKMC models

The method and the models available in the LAKIMOCA code are described in detail elsewhere [31]. Briefly, defects are treated as objects with specific positions in a simulation volume. Probabilities for physical transition mechanisms are calculated based on Boltzmann factor frequencies. After a certain event is chosen, time is increased according to a residence time algorithm [66]. The basic aspects of the parameterization used are described in [31]. The three parameter sets used here differ from each other in the treatment of SIA and SIA cluster mobilities. In set I, all SIA clusters (size $m \geqslant 2$) migrate in 1D, with a migration energy $E_m = 0.04$ eV and a prefactor decreasing with size according to the law: $v_0 \cdot m^{-s}$ ($v_0 = 6 \times 10^{12}$ s^{-1}, $s = 0.51$, following Ref. [67]). In set II, small clusters ($m < 5$) migrate in 3D with $E_m = 0.4$ eV, as suggested by recent ab initio calculations [68], while larger clusters maintain 1D motion with $E_m = 0.04$ eV. For large clusters the prefactor decreases with $s = 0.51$ and for small ones it decreases with $s = 10$. Finally, set III treats small clusters ($m < 5$) in the same way as set II, but assumes that larger clusters are completely immobile (see Table 2). For vacancy clusters, the same mobility was used in all three sets: a migration energy of 0.65 eV and a prefactor decreasing with size according to the law $v_0 p^{-(m-2)}$ for $m \geqslant 2$ with $p = 100$ and $v_0 = 6 \times 10^{12}$. These sets are summarized in Table 2.

A damage rate of 10^{-6} dpa/s was simulated in the OKMC by injecting displacement cascades selected at random from the chosen cascade group until 0.1 dpa was reached, according to the so-called NRT relation [69]. This damage rate is typical of high-flux reactor operating conditions. The simulations were performed in a $200a_0 \times 200a_0 \times 200a_0$ volume, using periodic boundary conditions and a grain size of approximately 2 μm. The irradiation temperature was 340 K. With all sets, 100 ppm traps for single SIAs and SIA clusters (binding energy 0.65 eV, capture radius 0.5 nm) were included. This was necessary because of the generally high mobility of SIA clusters in sets I and II; they can only accumulate in the material if traps exist. These traps can be interpreted as the effect of impurities, such as C or N atoms, or even substitutional atoms, which are known to affect point defect motion due to their binding energy with SIA and vacancies. However, in the present model, impurity atoms do not appear explicitly; rather, *generic*, immobile traps that act on SIAs are included. No traps for single vacancies or vacancy clusters were included. This choice, as well as the choice of trap density, binding energy and capture radius was made because it has been demonstrated [31] that this simple parameter set was sufficient to reproduce the density of vacancy clusters (of any size) at different doses after neutron irradiation observed in the experiment of Eldrup and co-workers [70].

Table 2
Summary of parameter sets for the description of SIA cluster mobility

SIA cluster size (E_m, eV)	Set I			Set II			Set III		
	s	E_m	D	s	E_m	D	s	E_m	D
$m = 1$	–	0.3	3D	–	0.3	3D	–	0.3	3D
$2 < m < 5$	0.51	0.04	1D	10	0.4	3D	10	0.4	3D
$m \geqslant 5$	0.51	0.04	1D	0.51	0.04	1D	Immobile		

4. Cascades analysis methods

4.1. Detecting Frenkel pairs

In the BCA, a Frenkel pair is easily identified as a displaced atom which escaped recombination and the closest vacant lattice site. Its detection is thus straightforward. The situation is a little more ambiguous in MD cascades where lattice distortions are possible as well as local rearrangements involving several atoms, such as dumbbell interstitials, crowdions, dislocation loops, etc. Two approaches are currently used for detecting interstitials and vacancies in MD cascades, both of which are based on the occupancy of a given volume centred on a lattice site. In one case this volume is a Wigner–Seitz cell and in the other a spherical volume of specified radius (currently $0.3a_0$ in iron). Both methods have been applied in the previously published work on the displacement cascades listed in Table 1.

If either the Wigner–Seitz cell or the spherical volume is empty, the lattice site is considered to be a vacancy. If it contains two atoms, one interstitial is counted. The latter can be described as a dumbbell interstitial. Since the spheres do not fill all space, atoms that do not fall within one of the spheres are also interstitials. In order to compare

these methods, we estimated the number of Frenkel pairs using both for the LVP cascades. The results were close to identical confirming that, in the case of displacement cascades in iron, both methods are consistent with each other.

For simplicity, in the analysis of spatial point defect correlations that follows, the distinction between different types of interstitials (simple octahedral, dumbbells, crowdions) is ignored and all are simply designated as interstitials.

4.2. Estimating cluster populations

Point defect clusters occur when groups of point defects are formed within a small volume. Clusters are thus identified as groups of point defects having at least one other point defect within a distance shorter than some threshold value. This threshold distance is a parameter, here chosen as the second neighbor distance in iron. The resulting vacancy and interstitial clusters are then counted, as well as the percentages of vacancies and interstitials in clusters. Lists of clusters and of their positions are retained as input for OKMC simulations. In some cases, complexes that involve both vacancy lattice sites and interstitials are found. The difference between the number of SIA and vacancies determines cluster size and type in these cases.

The detection of clusters may differ slightly from one algorithm to another, depending on the treatment of dumbbells and crowdions in which no point defect location can be unambiguously assigned. For example, a dumbbell interstitial appears as two atoms nearly equidistant from a vacant lattice site. In the case of a dumbbell, it has been assumed that one atom in the pair, the closest to the shared vacancy, occupies it and the other is identified as a SIA. In the case of a crowdion (typically three atoms sharing two lattice sites), the interstitial location depends on the recombination sequence in the clustering algorithm. This may have minor consequences on cluster distributions, pair distance correlations and spatial distributions of point defects. The consequences on clustering were measured in the LVP and MLD cascades by using two different approaches with a second-neighbor criterion. In the first, the SIA is set at the centre of mass of the crowdion, while in the second the most distant atom from the shared vacancies is left as a SIA. It was found that this may lead to about a 10% divergence in some bins of the cluster size distributions (with a bin width of one point defect).

A second-neighbor criterion is here used for convenience. However, it has been suggested in [44] that it is not necessarily the most reliable one as far as SIAs are concerned. In that work, clustering algorithms were compared using either a third-neighbor criterion or by direct visualization of cluster motion during the animation of MD cascade evolution. A third-neighbor criterion was found to provide better agreement with the results based on visualization than the second-nearest neighbor. However, the cluster populations still differed from that determined by a visual approach when oscillations in crowdion configurations had to be accounted for.

4.3. Estimating pair separation distances

The most standard function for characterizing spatial correlations between atoms in infinite media is the pair correlation function, $g(r)$ (see e.g. [71]) where r is the vector pair distance. Given the small size of cascades and their irregular shapes, and disregarding angular correlations in the orientation of Frenkel pairs, it is convenient to use a pair distance correlation function (pdf) defined as

$$G(r) = \frac{1}{N(N-1)} \sum_{i=1}^{N} \sum_{j>i}^{N} \delta(r - r_{ij})$$

$$\text{where } G(r) = \frac{4\pi r^2}{\Omega} g(r) \tag{1}$$

and Ω is the volume. In a structure-less infinite homogeneous medium, $G(r)$ increases with r^2 while $g(r)$ is unity. $G(r)$ is normalized in such a way that

$$IG(R) = \int_0^R G(r)\mathrm{d}r \tag{2}$$

is unity when $R \geqslant r_{ij}^{\max}$, the largest separation distance between point defects in a cascade. The integral (2) will be used here to analyze pair separation distances between point defects in cascades over all distances within the simulations box.

4.4. Estimating spatial extents

Component analysis permits an ellipsoid to be associated with each individual displacement cascade, accounting for its spatial extension and its morphology on the basis of its intrinsic characteristics [72]. The information provided by this method is the direction of three orthogonal axes that are associated with the spatial point defect distribution and the variance of this distribution projected onto

them. The major axis has the direction maximizing the variance, α^2, while the second maximizes the variance β^2 of the distribution projected onto a plane perpendicular to the first and the third has the direction minimizing this variance, γ^2. These directions are parallel to the directions of the eigenvectors of the covariance matrix of the point defect distributions and the associated eigenvalues are the variances of the distribution projected onto the directions of the eigenvectors. The eigenvectors and eigenvalues naturally define the ellipsoid associated with each cloud of point defects, with axis lengths given by the standard deviation of the distributions projected in the directions of the eigenvectors. Such ellipsoids can be associated distinctly with sets of vacancies and of interstitials in each cascade, characterized by their volume and by an aspect ratio. The latter is here defined by

$$\lambda = \frac{\alpha}{\gamma} - 1 \tag{3}$$

and measures the offset from spherical symmetry.

5. Comparison after short term evolution

5.1. Cascades computed with the same code and different potentials

In [44], a comparison was already presented between sets of cascades generated using the DYMOKA code with four different potentials referred above as AMS, ABC, CWP and WOL. The approach has the advantage that cascades are calculated with exactly the same simulation strategy and that cascade properties are evaluated using the same methods and algorithms. Cascades were compared from 5 to 40 keV energy, using each potential, and differences in the evolution and in the final point defect configurations were analyzed. The full analysis will not be repeated here and the reader may refer to [44] for the details.

Only the final MD configurations of the 20 keV cascades from that work, generated in boxes of $50a_0$ size are reanalyzed here, for consistency with the approach used also for analyzing cascades from other sources. Table 3 provides the mean numbers of Frenkel pairs obtained and percentages of vacancies and SIA in clusters, with the associated standard errors on the mean (sem). The standard deviations of associated frequency distributions can be directly deduced from the sem and the number of cascades given in the same Table 3.

As already noticed in [44], and consistently with the early ballistic theories based on energy partition [73–75], the mean number of Frenkel pairs is not significantly potential-dependent and its frequency distribution around the mean is rather narrow (standard deviation of 10–20% of the mean). These distributions are known in the case of BCA cascades to be close to symmetrical [76] and narrow as well. In contrast, percentages of vacancies and interstitials in clusters display a much larger variability with $\delta \sim 100$ and $\delta \sim 50$ respectively. The reasons for this variation are difficult to determine because of the various competing processes involved. Clusters are formed directly during the ballistic phase of the cascades and, as found in [24,44], they may anneal or fragment, or grow further during the cooling phase. The fraction of ballistically-clustered point defects as well as the length of the cooling phase is strongly potential-dependent. The thermal diffusion that follows is also potential-dependent and may give rise to additional SIA clustering.

Clustered vacancy and SIA fractions obtained with the various potentials and models are shown

Table 3
Mean numbers of Frenkel pairs, percentages of vacancies and interstitials in clusters in a simulation box at initial 100 K equilibrium temperature, with standard errors on the mean

Cascades 20 keV	Number of cascades	$\langle \nu_{FP} \rangle$	sem	% Vacancy in clusters	sem	% Interstitials in clusters	sem
DMK (ABC)	10	48.7	2.071	17.7	1.6	33.1	1.8
DMK (CWP)	10	52.7	1.915	29	4.5	23.7	4.9
DMK (WOL)	10	50.1	2.562	41.4	4.2	42.0	3.9
DMK (AMS)	10	48.2	2.894	50.1	2.5	37.7	3.1
δ		9*		95		55	

DMK stands for cascades generated with DYMOKA. In the last row, δ measures the largest relative difference (in percent) between the mean numbers of Frenkel pairs, percentages of vacancies and of interstitials in clusters. It is defined for a quantity x by $\delta = 200\{\max(x) - \min(x)\}/\{\max(x) + \min(x)\}$. An asterisk is displayed when this difference is not significant with regard to the sem.

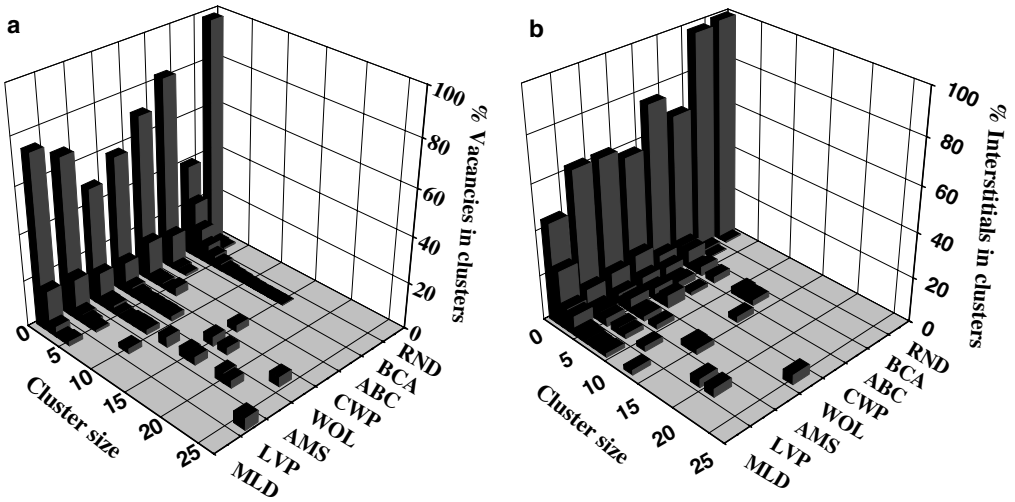

Fig. 1. Comparison of the size distributions of percentages of (a) vacancies and (b) interstitials in clusters calculated with DMK with different potentials, with LVP and the AMS potential, with MLD and the FS potential and with BCA and the ZBL potential. The size distributions obtained in random point defects distributions (RND) are shown for comparison. The cascade energy is 20 keV and the initial equilibrium temperature is 100 K.

in Fig. 1. The consequence of the models will be discussed in the next section. Here, we focus on the role of potentials, namely ABC, CVP, WOL and AMS. Consistent with the small standard deviations deduced from Table 3, the corresponding distributions are sharply peaked at the size of mono-vacancies and mono-interstitials. However, they display tails toward large cluster sizes with lengths partially correlating with a decrease of mono-defect frequencies. The samples are too small to allow for statistical analysis of the skewness of the distributions in Fig. 1. However, the results in this figure are qualitatively consistent with skewness being sensitive to the potential. Whether this may correlate with the long-term evolution of point defect clusters is examined in Section 6.

Spatial extent data are summarized in Table 4. Distributions of volumes associated with vacancies as well as with interstitials are known to be quite broad, with the consequence of large sem values and thus of large standard deviations (from 50% to 100% of the mean). On top of this dispersion, vacancy volumes are significantly potential-dependent with δ above 100. SIA volumes are not as sensitive to the potential. A δ-value of 25 is found, which, despite its magnitude, is not statistically significant according to the criterion employed. Again, a straightforward relation between the potential characteristics and the spatial extent of vacancies is difficult to determine and the analysis of this problem is beyond the scope of the present report. The aspect ratios of the interstitial component of cascades for the different potentials are not statistically different. Hence, the model potential affects the cascade volume, and thus the point defect density, and the mean cascade elongations as well. Interstitial distributions are less elongated than vacancy distributions.

Table 4
Mean volumes of vacancy and interstitial ellipsoids, aspect ratios of vacancy and interstitial distributions in a simulation box at 100 K initial temperature, with standard errors on the mean

Cascades 20 keV	$\langle\Omega_{VAC}\rangle$	sem	$\langle\Omega_{INT}\rangle$	sem	λ_{VAC}	sem	λ_{INT}	sem
DMK (ABC)	1024	168	4010	532	2.41	0.1	1.05	0.10
DMK (CWP)	1620	508	5142	698	2.97	0.7	0.89	0.14
DMK (WOL)	621	166	4396	787	4.01	1.0	0.95	0.145
DMK (AMS)	460	108	4257	655	4.01	0.97	0.845	0.09
δ	111		25*		50		22*	

In the last row, δ is defined as in Table 3 and only accounts for DMK results.

5.2. Cascades with different potentials and codes

We now proceed to a comparison of sets of cascades calculated by different research groups using different codes and potentials. In this comparison, variability resulting from simulation strategies and from potentials cannot be distinguished.

In addition to full MD codes, the BCA MARLOWE code is also employed. A vacancy–interstitial recombination radius of $3.5a_0$ was determined to be necessary in order to match the predicted mean number of FP to the value obtained with DMK (SP) for 10 keV cascades at 600 K. The pertinence of this approach is discussed elsewhere [24]. Random uniform point defect distributions (RND) were also constructed. They will serve as a reference for examining the magnitude and the consequence of the internal structure of cascades in the long term. For building these distributions, coordinates of point defects were selected at random in ellipsoids such that the projected variances were equal to the mean projected variances of DMK cascades obtained with the ABC potential and generated in a box with 100 K initial temperature. The numbers of point defects of each kind were also adjusted on the same basis. Frenkel pairs and point defect cluster results are collected in Table 5 for 20 keV cascades, but the following discussion also applies to 5 and 10 keV cascades.

A decrease in the number of FP produced with increasing temperature is predicted by LVP, BCA, and MLD, although the differences in MLD results are at the limit of statistical significance. This decrease is not clearly energy dependent but its magnitude depends on the model. The fact that the δ-value obtained in the BCA is similar to that obtained by MD suggests that the effect of temperature, if any, occurs in the ballistic phase. This is consistent with a decrease of the length of replacement sequences with increasing temperature.

The comparison between LVP and MLD numbers of FP shows that differences in MD models induce differences at least equal to temperature effects. In the previous section, mean numbers of FP were found to vary less than 20% when changing the potential in the same code. The differences found in Table 5 may thus have part of their origin in the different simulation strategies adopted using the different codes.

The comparison with RND results clearly demonstrates that in both BCA and MD cascades, the clustering of vacancies and of interstitials after recombination is far from random. A comparison between BCA and MD results shows SIA clustering to be dominated by the post-ballistic evolution. How nascent vacancies and interstitials evolve after the ballistic phase is not known exactly and is probably potential-dependent too. The high recoil density [77] in the cascade local heat transport and the transient stress gradients at the interface between the cascade and its unperturbed surrounding may combine to enhance or decrease the point defect mobility and clustering. The population of vacancies in clusters follows from a balance between ballistic clustering and cluster dissolution during the cooling phase. Interstitials carried outward from the cascade core may cluster during either phase. The significant increase of the percentage of

Table 5
Numbers of Frenkel pairs and percentages of point defects in clusters

Cascades 20 keV	No. of cascades	$\langle \nu_{FP} \rangle$	sem	% V in clusters	sem	% I in clusters	sem
LVP 100 K	10	46.5	3.4	31.9	4.6	37.5	4.6
LVP 600 K	20	38	1.8	44.8	3.1	57.5	2.8
DMK 600 K	4	41	3	30.5	7.25	8.9	1.5
MLD 100 K	10	60.2	2.8	25.6	2.1	55.3	2.4
MLD 600 K	8	55.75	2.1	20.6	2.8	74	2.8
BCA 100 K	1000	61.075	0.16	60	0.27	1.85	0.08
BCA 600 K	1000	51.17	0.13	55	0.29	1.89	0.08
RND	10	46.8	2.1	1.6	0.8	0.4	0.4
δ_T(LVP)		20		33		42	
δ_T(MLD)		7.8*		21.6		29	
δ_T(BCA)		17.6		9		2*	
δ_C(LVP–MLD)		$26^{(100\,K)}$ $38^{(600\,K)}$		$22^{(100\,K)}$ $74^{(600\,K)}$		$38^{(100\,K)}$ $25^{(600\,K)}$	

δ-Values are given for differences obtained with different initial temperatures (δ_T) in LVP, MLD and BCA cascades. It is also given for differences between LVP and MLD cascades with 100 K initial temperature (δ_C).

vacancies in clusters with temperature in LVP cascades is not observed by MLD or BCA, leading to a higher divergence between LVP and MLD at the higher temperature (74%).

Although higher than predicted in the BCA, the percentage of SIA in clusters in DMK (SP) cascades is strikingly lower than in LVP and MLD, while the number of FPs and percentage clustered vacancies are intermediate. We found this difference to be specific to the clustering analysis method. In Table 5, a second-nearest neighbor (2nn) criterion is used. Using a 3nn criterion, it is found that the fraction of vacancies in clusters only increases by a few percent with all potentials considered. Second-neighbor vacancies are indeed stable configurations. In contrast, configurations of second-neighbor interstitials are predicted to be unstable with the SP potential and 3nn configurations are highly preferred. As a consequence, 3nn clustering leads to much higher fractions of interstitials in clusters, namely 42%, and remains almost unchanged when a 4nn clustering criterion is used. With the SP potential used in DMK, a 2nn criterion may thus appear too restrictive for properly describing the clustering of interstitials. Such sensitivity was not found in the other cascade data sets.

Spatial extent data are summarized in Table 6 for 20 keV cascades but the discussion below also applies to 5 and 10 keV results. As in Section 5.1, the most striking feature is the difference found in cascade volumes with different codes. Since the magnitude of this difference is similar as well, it may be assigned principally to the different potentials used. The standard deviations of MLD cascade volume distributions is also found strikingly higher than others. The effect of the initial temperature is unclear. It is not significant on the vacancy volume distributions – although a trend to increase with temperature is systematic – while mean interstitial volumes are predicted to decrease with increasing temperature in LVP, which is not contradicted by MLD nor by BCA. As in the previous section, all models predict vacancy volumes to have higher aspect ratios than interstitial volumes.

The point defect separation distances may correlate at distances longer than the strict 2nn, 3nn or 4nn criterion used to define clusters. Pair distance distribution functions (pdf) reveal information about the longer-range correlations between point defects. Fig. 2 shows the pdf for vacancy–vacancy (V–V), vacancy–interstitial (V–I) and interstitial–interstitial (I–I) pairs obtained for different sets of simulations of 20 keV cascades and for random point defect distributions. The range considered is over $40a_0$, which is close to the largest cascade size considered here. The pdf are seen to be influenced by the interatomic potential, the initial temperature and the cascade model well beyond the few first neighbor distances and the magnitude of the effect can be evaluated by comparing with the pdf measured in random point defect distributions. Every cascade model is characterized by pdf different from random, displaying pairs in excess at short distances (though larger than 2nn), while long-range correlations are never favored. This indicates an aggregation of point defects, which is more pronounced for homogeneous pairs (Fig. 2(a) and (c)) than heterogeneous pairs (Fig. 2(b)) and strongest within the shortest range for I–I pairs. The difference between homogeneous and heterogeneous pairs is not surprising. Close vacancy–interstitial pairs are likely to annihilate. At the same time, the vacancy and

Table 6
Mean vacancy and interstitial volumes, aspect ratios of vacancy and interstitial distributions

Cascades 20 keV	$\langle\Omega_{VAC}\rangle$	sem	$\langle\Omega_{INT}\rangle$	sem	λ_{VAC}	sem	λ_{INT}	sem
LVP 100 K	495	139	3100	322	3.8	0.8	1.3	0.2
LVP 600 K	542	94	1927	233	3.2	0.4	2.3	0.3
DMK 600 K	1405	299	3915	374	2.7	0.5	1.7	0.3
MLD 100 K	1835	390	5337	844	2.45	0.3	0.9	0.2
MLD 600 K	1986	536	5562	935	2.7	0.5	1.1	0.1
BCA 100 K	729	25.5	2626	46	4.29	0.10	1.60	0.03
BCA 600 K	825	21.1	2526	42	4.69	0.11	1.98	0.04
δ_T(LVP)	9*		46		16*		56	
δ_T(MLD)	8*		4*		9*		17*	
δ_T(BCA)	12		4		9		21	
δ_C(LVP–MLD)	$115^{(100\,K)}$		$53^{(100\,K)}$		$43^{(100\,K)}$		$35^{(100\,K)}$	
	$114^{(600\,K)}$		$97^{(600\,K)}$		$18^{*(600\,K)}$		$73^{(600\,K)}$	

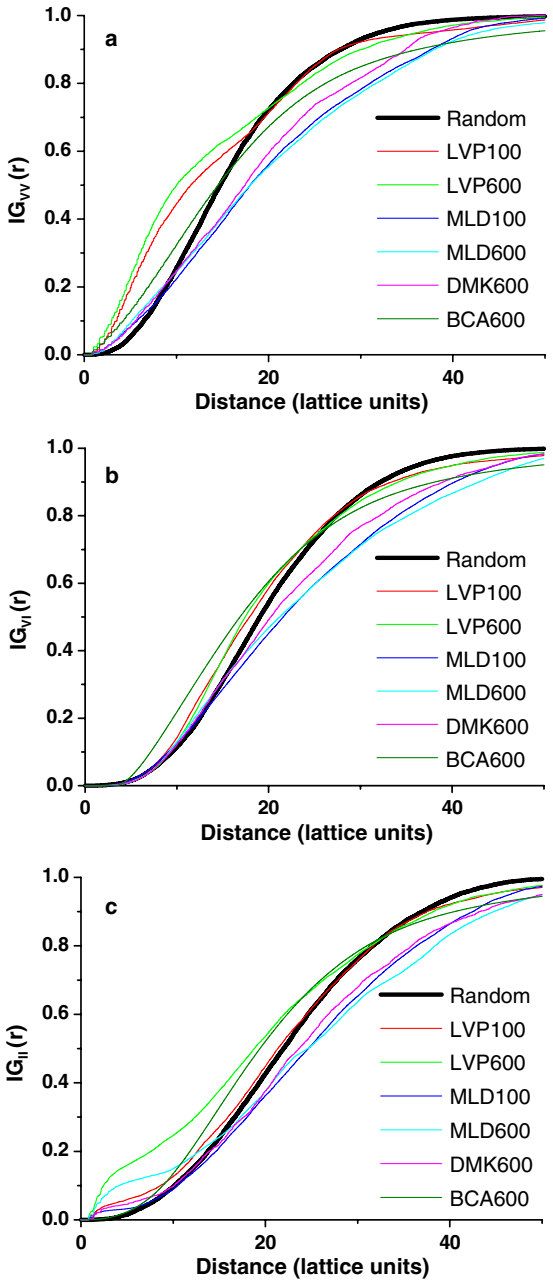

Fig. 2. Integrated pair distribution functions: (a) vacancy–vacancy, (b) vacancy–interstitial, (c) interstitial–interstitial. The cascade energy is 20 keV. The results are shown for LVP and MLD using initial boxes at 100 K and 600 K, DMK (SP) at 600 K and BCA at 600 K. The pdf are compared with the pdf in random point defect distributions to illustrate the occurrence of long distance correlations.

interstitial populations tend to be physically separated. (According to the cascade picture in [78], radial point defect distribution functions show vacancies dominantly in the core of cascades and interstitials at the periphery [24].) Therefore, small vacancy–interstitial separations are infrequent. The interaction between point defects may be appreciated by comparing MD and BCA results; the latter are only influenced by short-range repulsion between atoms during the ballistic phase. Comparing LVP or MLD results obtained with 100 K and 600 K initial temperatures shows this interaction to be thermally stimulated. The closest aggregation is found for interstitial–interstitial pairs, consistently with the 2nn clustering. Interstitials form no clusters in the BCA cascades. However, by comparing with the pdf for random interstitials distributions, the BCA interstitials are shown to be closer to each other, which is evidence for aggregation subsequent to ballistic interactions. The strength of aggregation is sensitive to the potential, although no systematic trend shows up.

Hence, like clustering (2nn–4nn), the longer-range correlation also appears to result from several processes that are both potential- and temperature-dependent and take place during both the ballistic and the cooling phases of the cascades.

6. Long-term evolution

In this section, we address the question of the possible influence of the differences pointed out in the previous paragraphs on the long-term evolution of the damage. As described above, the cascades used as input were obtained either with the same code, the same box size and different potentials or different codes, different box sizes and different potentials.

The cascades were periodically injected in the simulation box in order to model a rate of damage production of 10^{-6} dpa/s NRT, and the simulation was stopped as soon as a dose of 0.1 dpa NRT was reached. Given the limited OKMC box size (cubic with edges of $200a_0$), injecting one cascade significantly modifies the overall defect cluster populations. Therefore, rather than using the values obtained at the end of the cascade that brought the dose to 0.1 dpa, the populations of vacancy and interstitial clusters averaged over the last 0.01 injected dpa are here considered as representative of long-term evolution. They were analyzed and an example of results is given in Table 7. Errors associated with the sampling of number densities over the last 0.01 dpa are typically less than 1%. The OKMC simulations were performed using the three interstitial mobility parameters sets. The

Table 7
Number densities of vacancies in clusters at the end of long-term evolution (after 0.1 dpa damage production)

		RND	BCA	ABC	CWP	WOL	AMS	LVP	MLD	δ_{MD}
V	SET I	11.1	23.88	48.21	51.22	86.41	77.89	72.9	106.7	75
	SET II	19.54	32.93	29.98	32.46	50.91	46.41	44.11	25.85	65
	SET III	129.8	328.0	302.5	417.1	536.6	585.3	443.5	309.3	64
I	SET I	0.42	0.35	0.26	0.29	0.26	0.28	0.28	0.22	27
	SET II	5.94	10.38	6.40	6.91	8.36	8.50	7.56	8.06	28
	SET III	129.7	326.2	303.7	416.8	534.9	583.1	443.1	309.4	63

Units are $10^{18}/cm^{-3}$. The data are given when 20 keV cascades are used as input. The initial MD temperature is 100 K. Results are given for vacancies (V) in the first three rows, then for interstitials (I). δ-Values are given in the last column, only accounting for OKMC results using MD cascades as input.

cascades injected are all selected in the categories discussed in the previous section and the results are displayed category by category.

Results obtained with random point defect distributions are all outside the range of the others. This shows the importance of the role of the internal structure of the cascades on the long-term evolution. However, the features of the internal cascade structure that drives the long-term evolution have not yet been identified. For instance, the percentage of clustered vacancies in BCA cascades is greater than in MD predictions (see Table 5). However, Table 7 shows that the number densities of clustered vacancies obtained in the long term with BCA cascades is lower than all MD results with OKMC parameters set I and intermediate with sets II and III. The internal cascade structure is a consequence of both the ballistic and the cooling phases, which cannot be differentiated after long-term evolution. More generally, it is possible to classify OKMC results obtained with each set of OKMC parameters according to number density. For instance, with parameter set II, the ranking of number densities of clustered vacancies is, in decreasing order: WOL–AMS–LVP–BCA–CWP–ABC–MLD–RND. The ranking of SIA cluster number densities with sets II and III is similar. This indicates that the ranking of cluster populations in the long term does not depend much on the OKMC parameterization over a range of SIA mobility parameters even though the number densities differ by more than 1 order of magnitude.

The displacement cascades used as input can be ranked in the same way on the basis of percentages of vacancies in clusters. In decreasing order, one obtains: BCA–AMS–WOL–LVP–CWP–MLD–ABC–RND. Using the percentages of clustered SIAs in the same way gives: MLD–WOL–AMS–LVP–ABC–CWP–BCA–RND. Other than the invariably low ranking of RND, no clear correlation between one of these two latter sequences and the corresponding ones in the long term is found. The percentages of clustered point defects in cascades are thus not sufficient to explain point defect cluster populations in the long term. If sets of cascades are ranked by order of decreasing vacancy volumes, one obtains MLD–CWP–ABC–BCA–WOL–LVP–AMS, and by ranking interstitial volumes, MLD–CWP–WOL–AMS–ABC–LVP–BCA. Again, these sequences display no obvious correlation with the ranking of clustered number densities found in the long term.

It is possible to characterize the variability between cluster populations in the long term in the same way as was done for cascades in the previous section, using δ-values. Minimal and maximal number densities of point defects in clusters can be derived from Table 7.

The results are shown in Table 7 for the three mobility parameter sets employed in the OKMC. As far as vacancies are concerned, no large difference in the δ-values is found. This is consistent with the fact that the mobility parameters for vacancies and vacancy clusters are the same in the three parameter sets. The value $\delta_V \sim 68\%$ is somewhat smaller than the values for the clustered fraction in displacement cascades (95% in Table 3), though of the same order. The variability in SIA clustering is highest with the lowest mobility model. With the intermediate mobility parameterization (set II), the δ-value of clustered interstitial number densities is a little smaller than the δ-value of the clustered interstitials in the displacement cascades (55% in Table 3). It is notable that, despite the order of magnitude difference between number densities obtained with sets I and II, the variabilities obtained are the same. It is only when large clusters are immobile (set III) – and so cannot be absorbed at grain

Table 8
Same as Table 7, using cascades generated in boxes with different initial temperatures

		BCA 600 K	BCA 100 K	LVP 600 K	LVP 100 K	MLD 600 K	MLD 100 K	DMK 600 K
V	SET I	188.0	238.8	917.6	729.0	130.0	106.7	210.6
	SET II	282.7	329.3	65.31	44.11	59.11	35.85	19.32
	SET III	246.5	328.0	539.0	443.5	486.0	309.3	185.8
I	SET I	0.371	0.352	0.180	0.278	0.188	0.219	0.341
	SET II	9.265	10.38	5.716	7.561	6.734	8.062	6.008
	SET III	245.0	326.2	538.7	443.1	488.1	309.4	186.8

boundaries – that the variability is significantly enhanced.

The effect of the initial cascade box temperature at the end of a long-term evolution can be seen in Table 8.

The same temperature of 340 K is used in the OKMC so that differences in the results are only the consequence of differences in the initial displacement cascade structures induced by the initial box temperature. With all sets of OKMC parameters, the results obtained with MD cascades predict an increase of the number density of vacancies in clusters with temperature while the opposite is predicted with BCA cascades. This is another indication that, qualitatively, populations of vacancies in clusters are not affected by the parameterization of the SIA cluster mobility. The result also shows that, while LVP and MLD data yield opposite behavior of clustered vacancy fractions with temperature in displacement cascades (Table 5), the same trend is found in the long term, contrary to the BCA sets. This illustrates the lack of obvious relationship between the clustering properties of vacancies in the short and long term.

As far as interstitial clustering is concerned, the consequences of temperature predicted by LVP and MLD correlate as well. Number densities decrease with increasing cascade box temperature, except with the lowest mobility parameter set where the opposite is found. Using BCA cascades, a trend of decrease is predicted with increasing temperature and all mobility sets. Again, no obvious relationship shows up in the temperature dependence of clustered interstitial fractions at the end of displacement cascades.

7. Synthesis

The damage created in displacement cascades calculated independently by different groups of researchers using different models has been compared and characterized statistically on the basis of several parameters. Differences emerged and were quantified. The objective was to address the possible consequences of these differences on long-term cluster growth.

The largest difference in models used to generate cascades lays between the group of full MD simulations and calculations computed in the BCA. By ignoring collective interactions, the BCA only models the ballistic phase of cascades which lasts for no more than a fraction of a picosecond, while typical evolution times used in MD simulations are well beyond 10 ps. In the BCA, it was necessary to assign a value to the parameter defining the vacancy–interstitial recombination threshold distance, regardless of the recombination mechanisms, in order to account in an approximated way for the cascade relaxation phase. The main consequence is a severe underestimation of the clustered SIA fraction and a less severe overestimation of the clustered vacancy fraction. Surprisingly, this difference has no dramatic consequence on the number density of clustered interstitials in the long term.

A second difference concerns MD cascades and the different interatomic potentials used in the simulations. Using a single code (DMK) and simulation strategy, it was possible to determine the consequences of different potentials on displacement cascade characteristics and the long-term damage evolution. Differences in the vacancy and the SIA clustered fractions were significant (95% and 55% respectively). However, in the long term, no correlation could be established between these fractions and the number densities of clustered vacancies and SIAs.

A third difference between the primary damage models is the temperature of the system in which cascades are generated. Except in the BCA, constant temperature was not imposed on the simulation boxes. This results in an increase in box temperature at the end of the cascades, which is box-size

dependent but not significantly dependent on the initial temperature. Therefore, initial temperature effects for a given cascade energy were measured for boxes of the same size and thus at constant bias. In all models, increasing the temperature has the consequence of decreasing the number of Frenkel pairs, suggesting the effect to be ballistic. Changes in point defect clustered fractions are more significant. Increasing the temperature enhances SIA clustering. Results of vacancy clustering are not conclusive. As far as temperature is concerned, and similar to changes in potential, no clear correlation was found between point defect clustering in displacement cascades and the number densities in the long term.

These results suggest that point defect clustered fractions in cascades are not crucial parameters for long-term cluster growth, raising the possibility that the internal structure of cascades does not have a significant impact on the ultimate cluster evolution. The fact that no correlation was found between the spatial extent of cascades and the long-term evolution lends support to this speculation. However, this view is countered by the comparison of cluster populations obtained at 0.1 dpa when displacement cascades and when random (and hence statistically structure-less) point defect distributions with similar spatial extents. The comparison of pair distance distributions demonstrated spatial correlations in cascades at longer distances than those involved in point defect clusters, but their possible relation to the long-term cluster growth has not yet been examined.

A fourth difference between groups of cascades analyzed in this work is the computational strategy used in the MD codes for calculating them. This encompasses the management of time steps, integration schemes, boundary conditions and the total elapsed time. All these aspects may have an influence on the simulation results. To measure this influence would require systematic comparative simulations that are beyond the scope of this report.

Three different published sets of OKMC parameters have been used to investigate long-term evolution, and they result in orders of magnitude differences in number densities once the irradiation dose reaches 0.1 dpa. However, different cascade models do not induce differences of more than a factor of 2 in the long-term total number densities, suggesting that the results are more sensitive to the OKMC parameters. However, this factor of 2 may increase if the cluster populations are examined in deeper detail that was done here. For instance, differences in the predicted number densities of large clusters may be much larger than the differences in integral parameters such as the total number of point defects in clusters. Large clusters are particularly relevant to radiation-induced hardening and this points to the importance of carrying out more detailed studies of the possible correlation between the internal structure of displacement cascades and the evolution of the point defect cluster size distributions at higher doses.

Acknowledgements

This work was prepared in the framework of the integrated project PERFECT (F160-CT-2003-508840) under programme EURATOM FP-6 of the European Commission, on the basis of displacement cascades computed by the authors independently before and during the project. Research of Osetsky and Stoller was sponsored by the Division of Materials Sciences and Engineering and the Office of Fusion Energy Sciences, US Department of Energy, under contract DE-AC05-00OR22725 with UT-Battelle, LLC.

References

[1] https://www.fp6perfect.net/perfect.
[2] A.F. Calder, D.J. Bacon, J. Nucl. Mater. 207 (1993) 25.
[3] V.G. Kapinos, D.J. Bacon, Phys. Rev. B 50 (1994) 13194.
[4] V.G. Kapinos, D.J. Bacon, Phys. Rev. B 52 (1995) 4029.
[5] D.J. Bacon, T. Díaz de la Rubia, J. Nucl. Mater. 216 (1994) 275.
[6] W.J. Phythian, A.J.E. Foreman, R.E. Stoller, D.J. Bacon, A.F. Calder, J. Nucl. Mater. 223 (1995) 245.
[7] R.E. Stoller, J. Nucl. Mater. 233 (1996) 999.
[8] F. Gao, D.J. Bacon, A.F. Calder, P.E.J. Flewitt, T.A. Lewis, J. Nucl. Mater. 230 (1996) 47.
[9] V.G. Kapinos, D.J. Bacon, Phys. Rev. B 53 (1996) 8287.
[10] R.E. Stoller, G.R. Odette, B.D. Wirth, J. Nucl. Mater. 251 (1997) 49.
[11] F. Gao, D.J. Bacon, P.E.J. Flewitt, T.A. Lewis, J. Nucl. Mater. 249 (1997) 77.
[12] F. Gao, D.J. Bacon, P.E.J. Flewitt, T.A. Lewis, Modell. Simul. Mater. Sci. Eng. 6 (1998) 543.
[13] D.J. Bacon, F. Gao, Yu.N. Osetsky, J. Comput.-Aided Mater. Des. 6 (1999) 225.
[14] R.E. Stoller, L.R. Greenwood, J. Nucl. Mater. 271 (1999) 57.
[15] C.S. Becquart, C. Domain, A. Legris, J.C. Van Duysen, J. Nucl. Mater. 280 (2000) 73.
[16] A.F. Calder, D.J. Bacon, Yu.N. Osetsky, in preparation.
[17] R.E. Stoller, J. Nucl. Mater. 276 (2000) 22.
[18] E. Alonso, M.J. Caturla, T. Diaz de la Rubia, N. Soneda, J. Marian, J.M. Perlado, R.E. Stoller, J. Nucl. Mater. 283 (2000) 768.
[19] R.E. Stoller, A.F. Calder, J. Nucl. Mater. 283 (2000) 746.
[20] R.E. Stoller, Nucl. Eng. Des. 195 (2000) 129.

[21] M. Hou, A. Souidi, C.S. Becquart, J. Phys. C13 (2001) 5365.
[22] F. Gao, D.J. Bacon, P.E.J. Flewitt, T.A. Lewis, Nucl. Instrum. and Meth. B 180 (2001) 187.
[23] C.S. Becquart, C. Domain, J.C. van Duysen, J.M. Raulot, J. Nucl. Mater. 294 (2001) 274.
[24] A. Souidi, M. Hou, C.S. Becquart, C. Domain, J. Nucl. Mater 295 (2001) 179.
[25] A. Souidi, A. Elias, A. Djaafri, C.S. Becquart, M. Hou, Nucl. Instrum. and Meth. B 193 (2002) 341.
[26] M. Hou, A. Souidi, C.S. Becquart, Nucl. Instrum. and Meth. B 196 (2002) 31.
[27] Yu.N. Osetsky, D.J. Bacon, B.N. Singh, B. Wirth, J. Nucl. Mater. 307 (2002) 852.
[28] D.J. Bacon, Y.N. Osetsky, R.E. Stoller, R.E. Voskoboinikov, J. Nucl. Mater. 323 (2003) 152.
[29] O. Khrushcheva, E.E. Zhurkin, L. Malerba, C.S. Becquart, C. Domain, M. Hou, Nucl. Instrum. and Meth. B 202 (2003) 68.
[30] R.E. Stoller, S.G. Guiriec, J. Nucl. Mater. 329 (2004) 1238.
[31] C. Domain, C.S. Becquart, L. Malerba, J. Nucl. Mater. 335 (2004) 121.
[32] L. Malerba, D. Terentyev, P. Olsson, R. Chakarova, J. Wallenius, J. Nucl. Mater. 329 (2004) 1156.
[33] J. Wallenius, I.A. Abrikosov, R. Chakarova, C. Lagerstedt, L. Malerba, P. Olsson, V.V. Pontikis, N. Sandberg, D. Ternetyev, J. Nucl. Mater. 329 (2004) 1175.
[34] D. Terentyev, L. Malerba, J. Nucl. Mater. 329 (2004) 1161.
[35] L. Malerba, C.S. Becquart, M. Hou, C. Domain, Philos. Mag. A 85 (2005) 417.
[36] C.S. Becquart, A. Souidi, M. Hou, Philos. Mag. A 85 (2005) 409.
[37] L. Malerba, J. Nucl. Mater. 351 (2006) 28.
[38] A. Barbu, C.S. Becquart, J.L. Bocquet, J. Dalla Torre, C. Domain, Philos. Mag. A 85 (2005) 541.
[39] M.W. Finnis, MOLDY6-A Molecular Dynamics Program for Simulation of Pure Metals, AERE R-13182, UKAEA Harwell Laboratory, Harwell, UK, 1988.
[40] M.T. Robinson, Phys. Rev. B 40 (1989) 10717.
[41] M.-J. Caturla, N. Soneda, E. Alonso, B. Wirth, T. Diaz de la Rubia, J.M. Perlado, J. Nucl. Mater. 276 (2000) 13.
[42] M.D. Johnson, M.J. Caturla, T. Diaz de la Rubia, J. Appl. Phys. 94 (1998) 1963.
[43] C.S. Becquart, A. Souidi, C. Domain, M. Hou, L. Malerba, R.E. Stoller, J. Nucl. Mater. 351 (2006) 39.
[44] D. Terentyev, C. Lagerstedt, P. Olsson, K. Nordlund, J. Wallenius, C.S. Becquart, L. Malerba, J. Nucl. Mater. 351 (2006) 65.
[45] C. Domain, C.S. Becquart, Phys. Rev. B 65 (2001) 024103.
[46] G. Simmons, H. Wang, Single Crystal Elastic Constants and Calculated Aggregate Properties: A Handbook, MIT, Cambridge, 1971.
[47] C.-C. Fu, F. Willaime, P. Ordejón, Phys. Rev. Lett. 92 (2004) 175503.
[48] C. Kittel, Introduction to Solid State Physics, 6th Ed., John Wiley, 1987.
[49] C. Domain, J. Nucl. Mater. 351 (2006) 1.
[50] L. De Schepper et al., Phys. Rev. B 27 (1983) 5257.
[51] K. Maier, H. Metz, D. Herlach, H.-E. Schaefer, J. Nucl. Mater. 69&70 (1978) 589.
[52] H.-E. Schaefer et al., Scr. Metall. 11 (1977) 803;
H. Matter, J. Winter, W. Triftshäuser, Appl. Phys. 20 (1979) 135.
[53] K. Fürderer et al., Mater. Sci. Forum 15–18 (1987) 125;
A. Seeger, Phys. Status Solidi A 167 (1998) 289.
[54] L.J. Cuddy, Acta Metall. 16 (1968) 23.
[55] T. Tabata et al., Scr. Metall. 14 (1983) 1317.
[56] C.H. Woo, W. Frank, Radiat. Eff. 77 (1983) 49;
F. Philipp, Mater. Sci. Forum 15–18 (1987) 187.
[57] F.S. Buffington, K. Hirano, M. Cohen, Acta Metall. 9 (1961) 434.
[58] V.M. Amonenko, A.M. Blinkin, I.G. Ivantsov, Phys. Met. Metall. 17 (1964) 54.
[59] G.J. Ackland, M.I. Mendelev, D.J. Srlolovitz, S. Han, A.V. Barashev, J. Phys. C 16 (2004) 1.
[60] M.W. Finnis, J.E. Sinclair, Philos. Mag. A 50 (1984) 45, and Erratum;
Philos. Mag. A 53 (1986) 161.
[61] G. Simonelli, R. Pasianot, E.J. Savino, Mater. Res. Soc. Symp. Proc. 291 (1993) 567;
This potential was used to design the Fe–Cu potential in, S.M. Ludwig, D. Farkas, D. Pedraza, S. Schmauder, Modell. Simul. Mater. Sci. Eng. 6 (1998) 19.
[62] G.J. Ackland, D.J. Bacon, A.F. Calder, T. Harry, Philos. Mag. A 75 (1997) 713.
[63] R. Chakarova, V. Pontikis, J. Wallenius, Development of Fe(bcc)–Cr many body potential and cohesion model, Delivery report WP6, SPIRE project, EC contract no. FIKW-CT-2000-00058, June 2002. Available at <www.neutron.kth.se/publications/library/DR-6.pdf; P. Olsson, L. Malerba, A. Almazouzi, SCKCEN Report, BLG-950, June 2003.
[64] J. Wallenius, P. Olsson, C. Lagerstedt, Nucl. Instrum. and Meth. B 228 (2005) 122.
[65] J.F. Ziegler, J.P. Biersack, U. Littmark, in: Stopping and Ranges of Ions in Solids, Pergamon, New York, 1985, p. 25.
[66] W.M. Young, E.W. Elcock, Proc. Phys. Soc. 89 (1966) 735.
[67] Yu. H. Osetsky, D.J. Bacon, A. Serra, B.N. Singh, S.I. Golubov, J. Nucl. Mater. 276 (2000) 65.
[68] F. Willaime, C.C. Fu, M.C. Marinica, J. Dalla Torre, Nucl. Instrum. and Meth. B 228 (2005) 92.
[69] M.J. Norgett, M.T. Robinson, I.M. Torrens, Nucl. Eng. Des. 33 (1975) 50.
[70] M. Eldrup, B.N. Singh, S.J. Zinkle, T.S. Byun, K. Farrell, J. Nucl. Mater. 307–311 (2002) 912;
M. Eldrup, B.N. Singh, J. Nucl. Mater. 323 (2003) 346.
[71] M.P. Allen, D.J. Tildesley, Computer Simulation of Liquids, Oxford Science Publishers, Oxford, 1987.
[72] M. Hou, Phys. Rev. B 31 (7) (1985) 4178.
[73] G. Leibfried, Bremstrahlungseffekte in Festkörpen, Teuben, Stuttgart, 1965.
[74] M.T. Robinson, Philos. Mag. 12 (1965) 741.
[75] P. Sigmund, Rev. Roum. Phys. 17 (1972) 823.
[76] M.T. Robinson, I.M. Torrens, Phys. Rev. B 9 (1974) 5008.
[77] P. Sigmund, Appl. Phys. Lett. 14 (1969) 144.
[78] J.A. Brinkman, J. Appl. Phys. 25 (1054) 961.